Electronic Supplementary Material (ESI) for Nanoscale.

Supporting information

Bifunctional Nanomodulator for Boosting CpG-Mediated Cancer Immunotherapy

Zhenzhen Wang, [a,b] *Yan Zhang,* [a,b] *Zhen Liu,* [a] *Kai Dong,* [a] *Chaoqun Liu,* [a,b] *Xiang Ran,*[a,b] *Fang Pu,*[a] *Enguo Ju,* [a,b] *Jinsong Ren**,[a] and *Xiaogang Qu**,[a]

[a] Laboratory of Chemical Biology and State Key Laboratory of Rare Earth Resources Utilization, Changchun Institute of Applied Chemistry, Chinese Academy of Sciences, Changchun, Jilin, 130022, P. R. China

[b] University of Chinese Academy of Sciences, Beijing 100039, P. R. China

*Address correspondence to jren@ciac.ac.cn; xqu@ciac.ac.cn

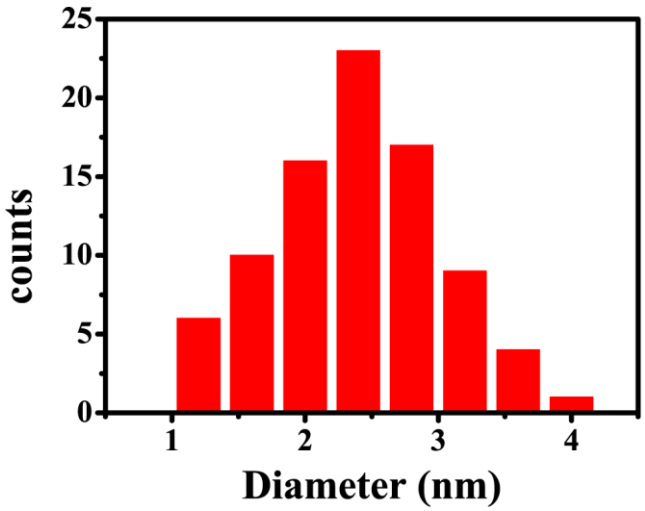

Fig. S1 Size distribution histogram of CpG-AgNCs nanoparticles.

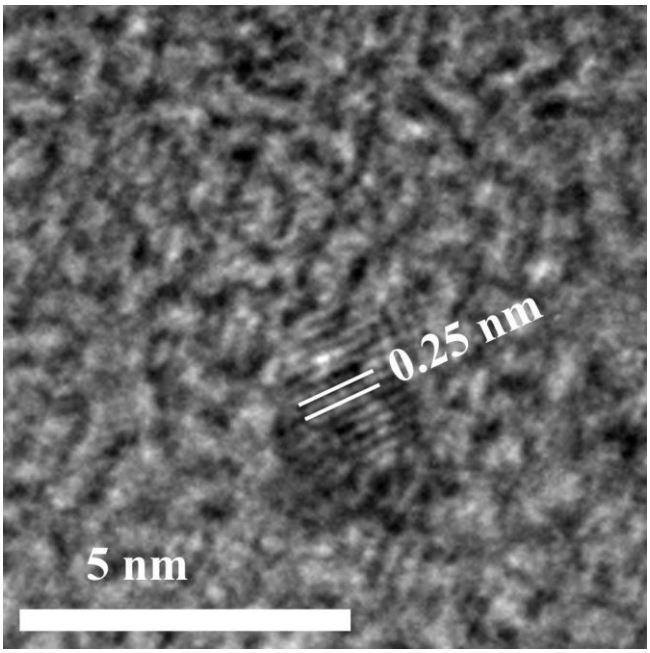

Fig. S2 The HRTEM image of CpG-AgNCs nanoparticles.

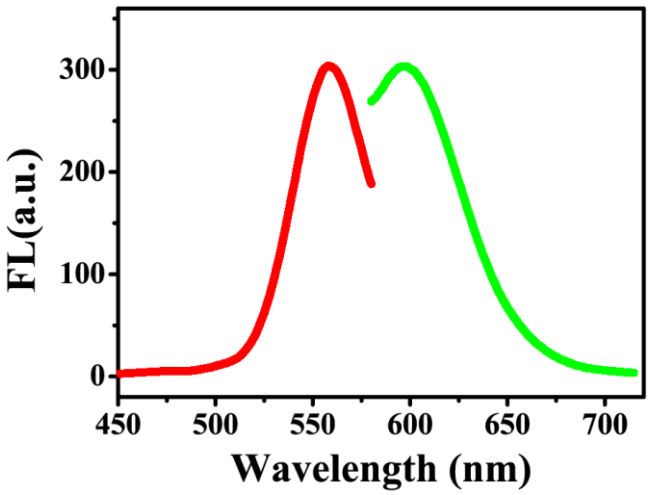

Fig. S3 Fluorescence excitation (red line) and emission (green line) spectra of CpG-AgNCs nanoparticles.

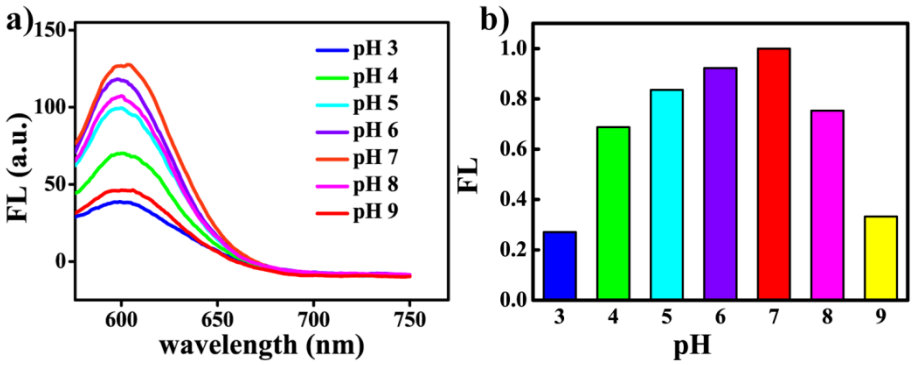

Fig. S4 Fluorescence emission spectra of CpG-AgNCs at different pH PBS buffer.

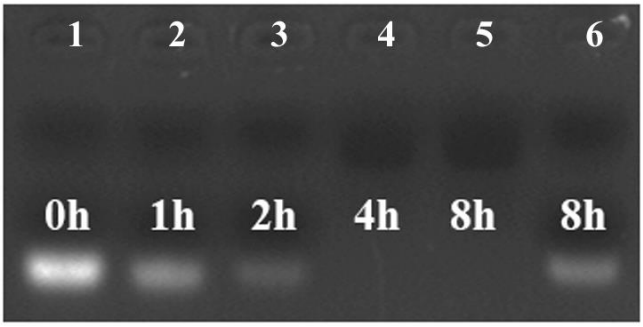

Fig. S5 Electrophoretic analysis of the stability of the CpG ODNs and CpG-AgNCs. The CpG ODNs were incubated with 50% non-heat-inactivated fetal bovine serum at 37 °C for 1-8 h (line 1-5). The line 6 was the CpG-AgNCs incubated with 50% non-heat-inactivated fetal bovine serum at 37 °C. We found that the CpG ODNs were almost completely degraded after 4 h incubation with 50 % non-inactivated fetal

bovine serum. In stark contrast, the band for CpG-AgNCs remained nearly unchanged after 8 h incubation under the same conditions, reflecting the high conformational stability of the CpG-AgNCs in biological media.

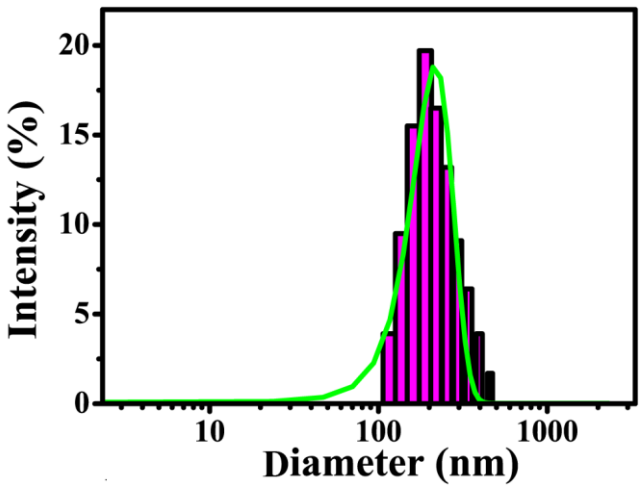

Fig. S6 The size distribution of MnO_2 nanosheets in water.

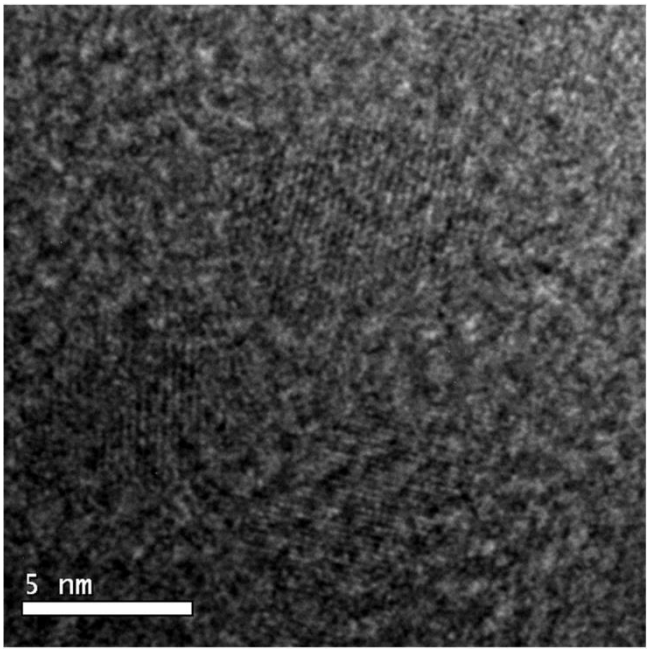

Fig. S7 The HRTEM image of MnO_2 nanosheets.

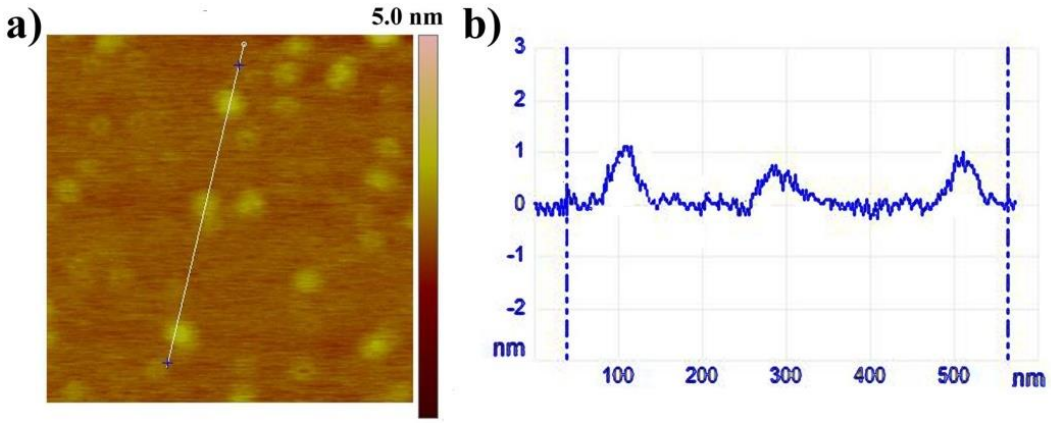

Fig. S8 a), b) AFM height image of MnO_2 nanosheets deposited on mica substrates.

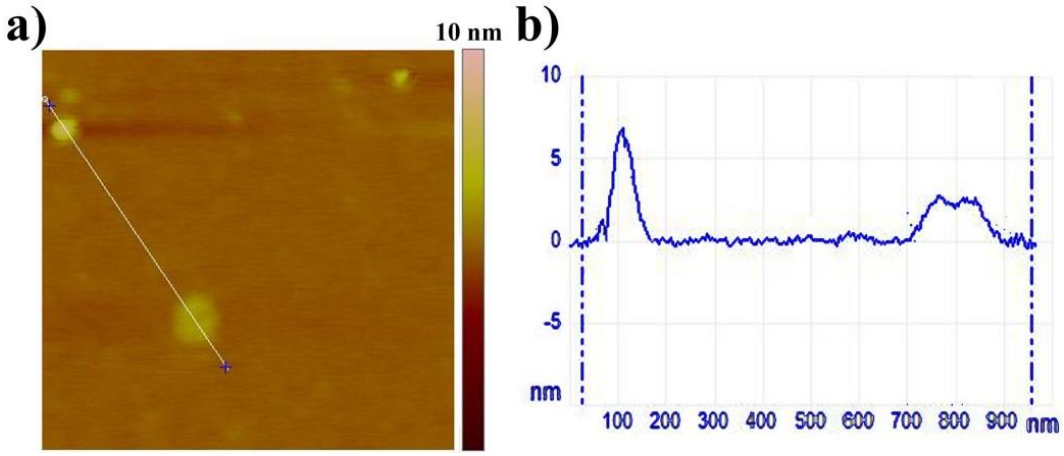

Fig. S9 a), b) AFM height image of MCA nanocomposites deposited on mica substrates.

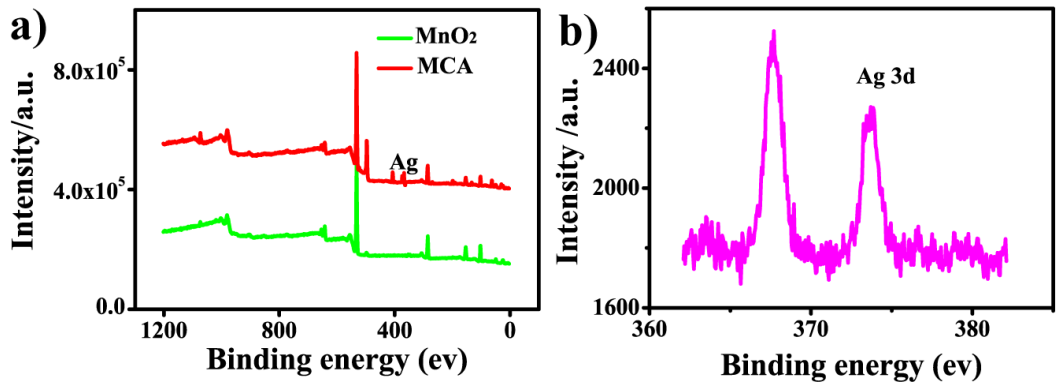

Fig. S10 a) X-ray photoelectron spectroscopy of MnO_2 nanosheets and MCA nanocomposites. b) The peaks assigned to Ag 3d.

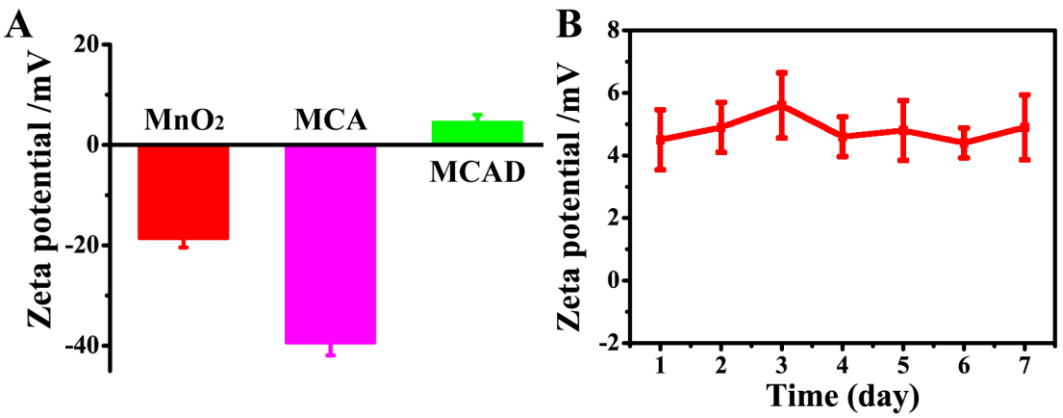

Fig. S11 A) The zeta-potential of MnO_2 nanosheets, MCA nanoparticles and MCAD nanocomposities. The surface of MnO_2 nanosheets was negatively charged with an average zeta potential of about -18.6 ± 1.8 mV. After the absorption of CpG-AgNCs nanoparticles, the resulting MCA nanocomplexes exhibited a higher negative zeta potential of about -39.4 ± 2.5 mV due to the strongly negative charge of DNA. Subsequently, during the absorption of DOX on the surface of MCA, the zeta potential changed from -39.4 mV to + 4.5 mV, indicating the successful preparation of MCAD nanocomposites. Such a relatively low zeta potential of MCAD nanocomposites would minimize an adsorption of proteins in blood vessels during prolonged circulation *in vivo*. B) Changes with time the zeta potential of MCAD in aqueous solution. As illustrated in Fig. S11, no obvious change in the zeta potential of MCAD nanocomposites was observed up to 7 days, indicating the good stability of MCAD nanocomposites.

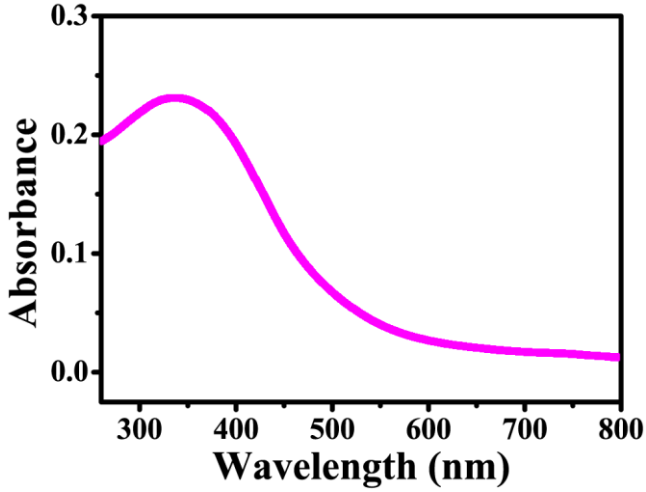

Fig. S12 UV-Vis absorption spectrum of MnO_2 nanosheets in aqueous solution.

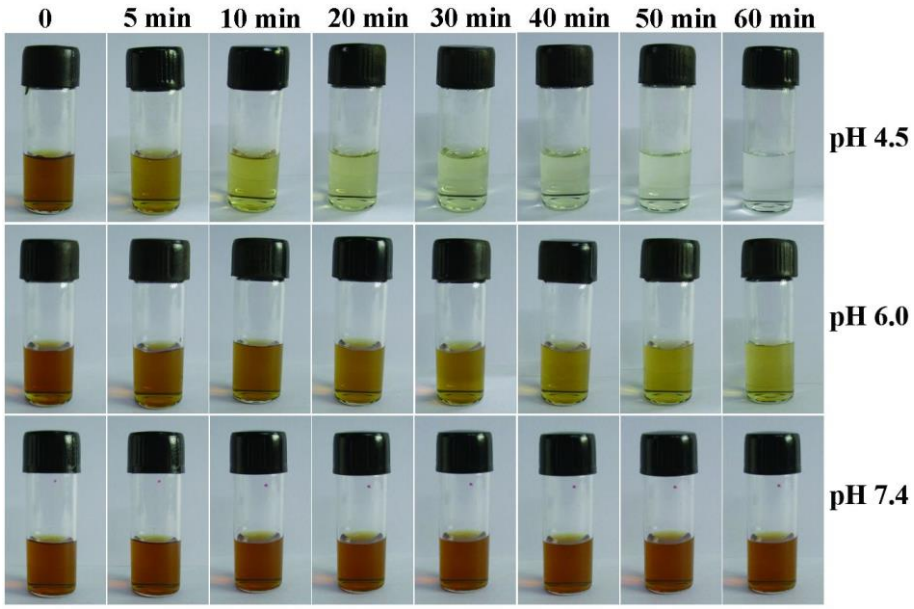

Fig. S13 Color changes and UV-Vis analysis of MnO_2 nanosheets after dispersed into buffer solutions with different pH values (4.5, 6.0 and 7.4) in a time course in the presence of H_2O_2 (50 μM).

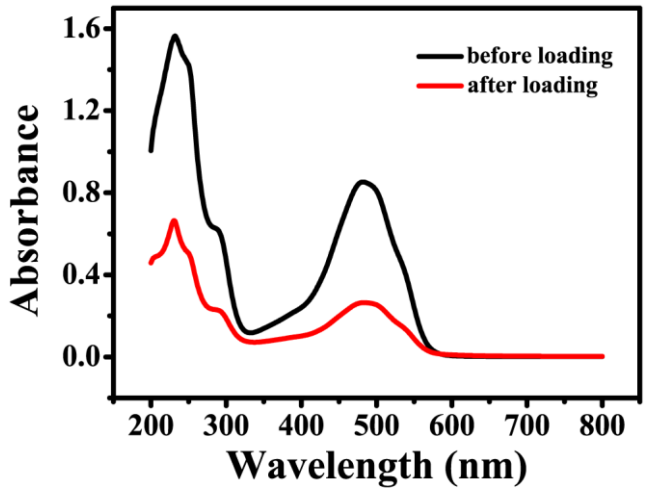

Fig. S14 UV-Vis absorption spectra of initial of DOX solution and supernatant DOX solution after mixing with MCA nanocomplexes.

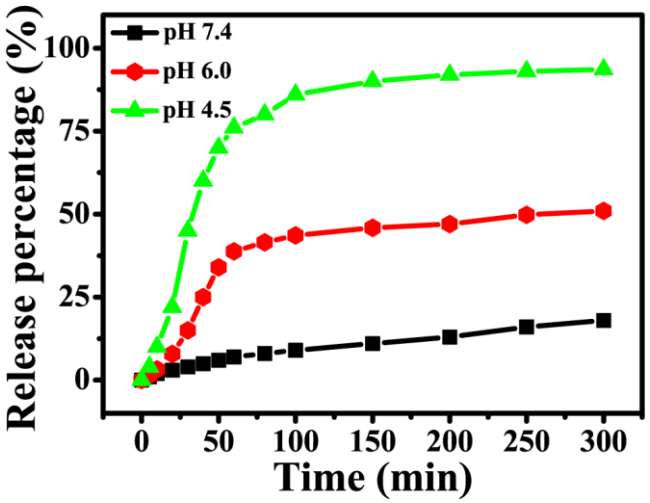

Fig. S15 The release percentage of DOX from MCAD nanocomposities in the presence of H_2O_2 at various pH values (pH = 7.4, 6.0, and 4.5). Owing to the pH/H_2O_2-responsive properties, MnO_2 nanosheets could be reduced into Mn^{2+} ions by acidic H_2O_2, thereby resulting in the release of DOX. As illustrated in Fig. S15, when H_2O_2 and H^+ presented, nearly 90% of DOX was released.

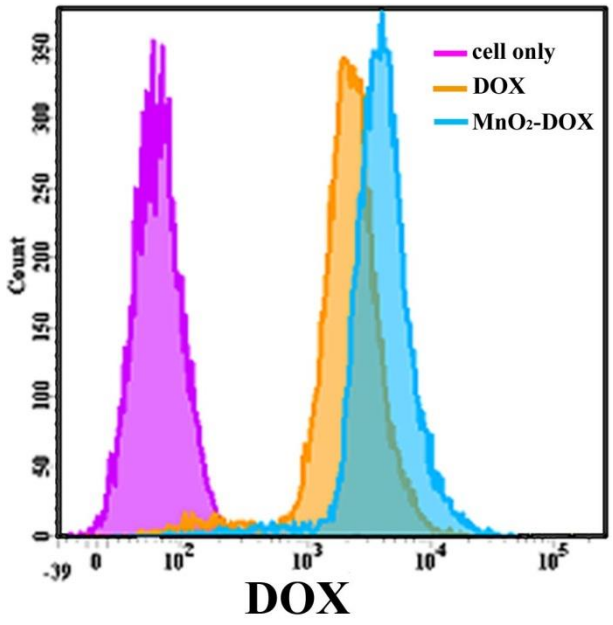

Fig. S16 Flow cytometry measurement of internalized DOX signals in 4T1 cells incubated with DOX and MnO_2-DOX respectively. Compared with free DOX, the 4T1 cells treated with MnO_2-DOX presented significantly higher fluorescence intensity, revealing that MnO_2 nanosheets could improve the cellular uptake of DOX and release it efficiently.

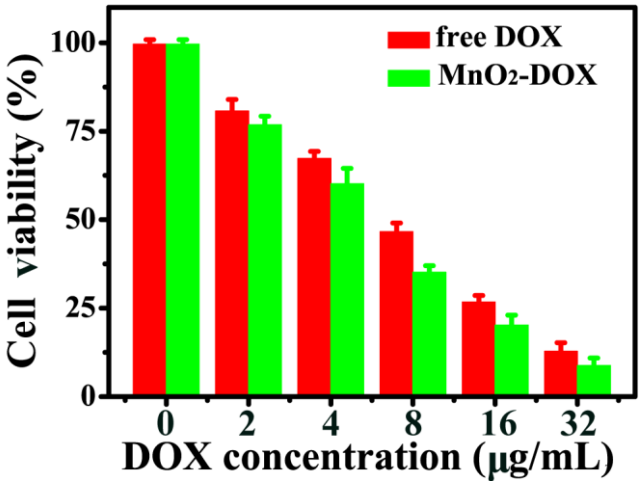

Fig. S17 The cell viability of 4T1 cells incubation with different concentrations of free DOX and MnO_2-DOX.

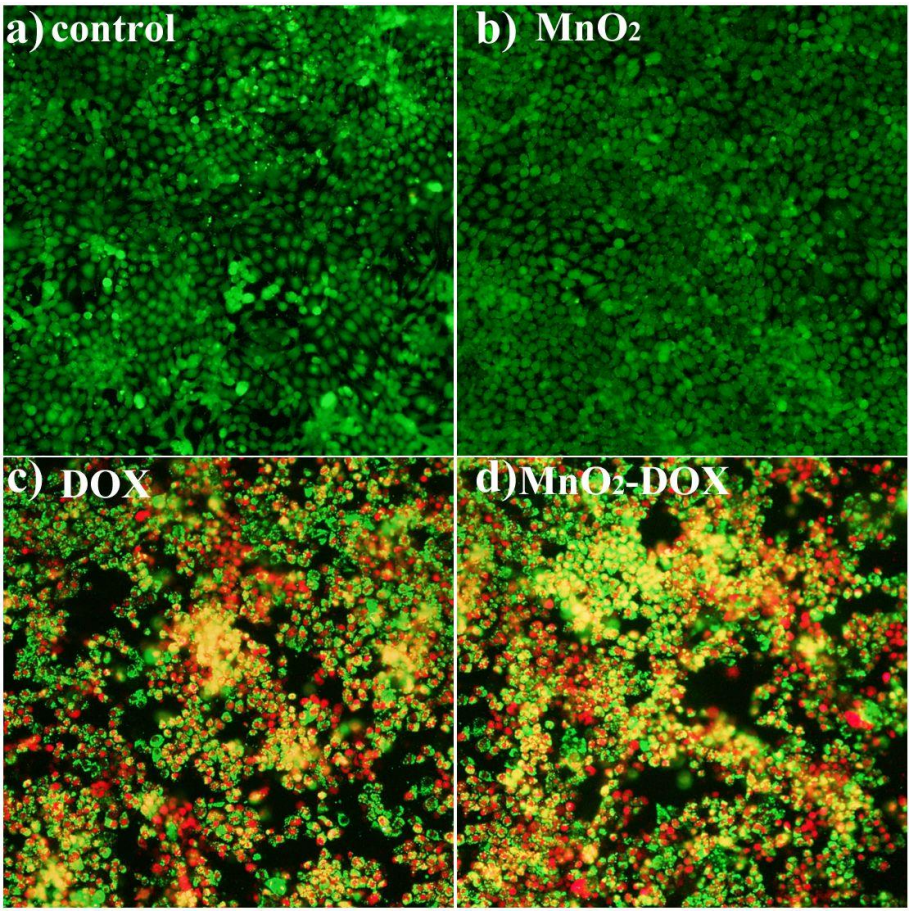

Fig. S18 The live/dead stain of 4T1 cells incubated with MnO_2 nanosheets, free DOX and MnO_2-DOX nanocomplexes.

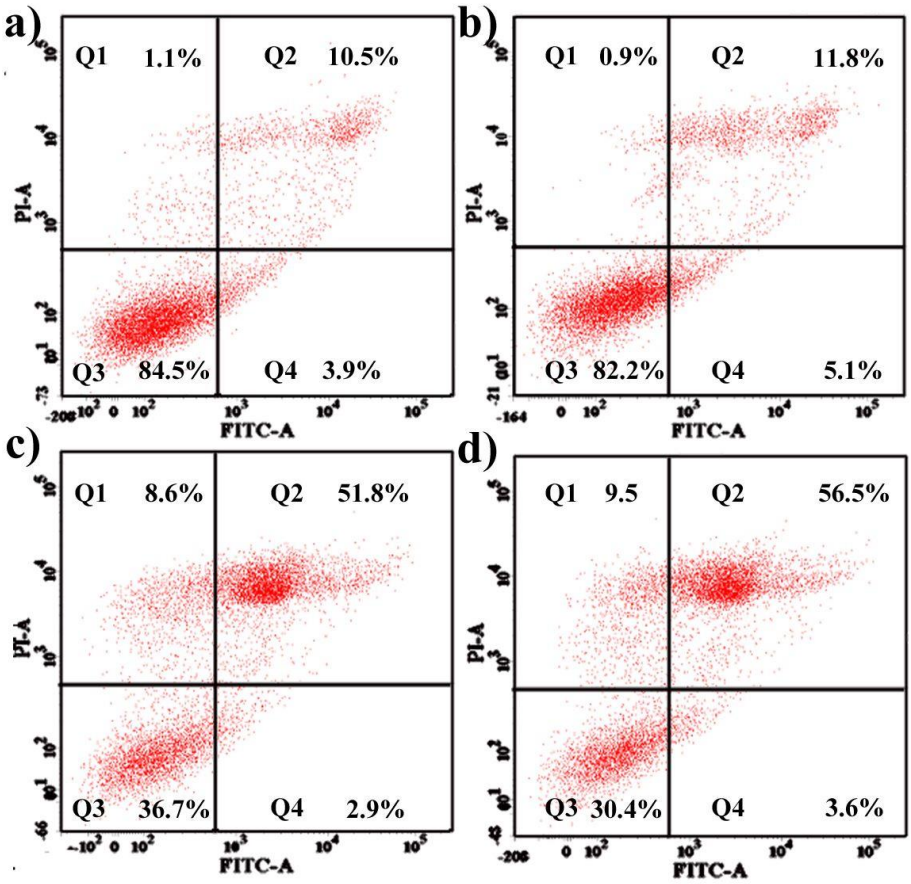

Fig. S19 Flow cytometry representing apoptosis assay based on Annexin V-FITC and PI staining of 4T1 cells. a) Control cells, b) MnO_2 nanosheets, c) free DOX, d) MnO_2-DOX nanocomplexes.

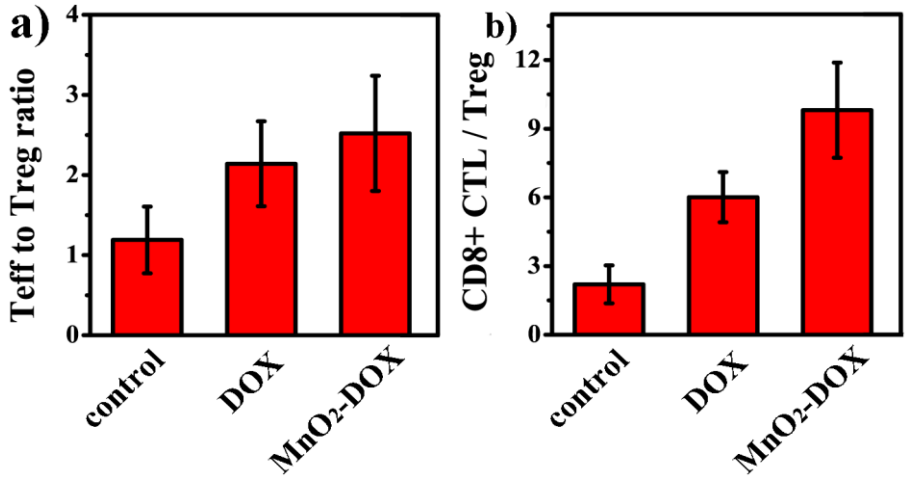

Fig. S20 Ratios of tumor-infiltrating effective $CD4^+$ T cells (a) and $CD8^+$ T cells (b) over regulatory T cells in tumors upon various treatments. Both ratios were significantly enhanced after DOX treatment.

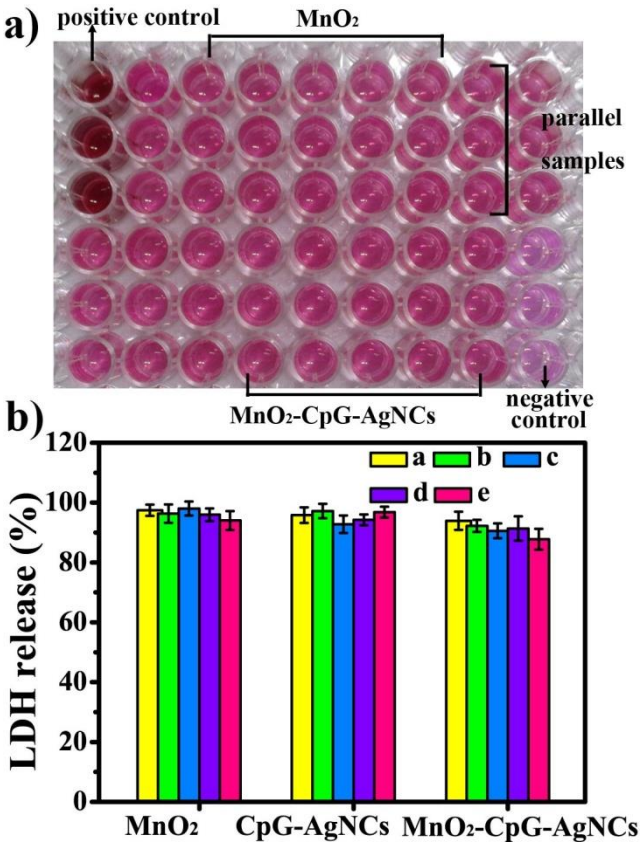

Fig. S21 a) Image of the toxicity of CpG-AgNCs, MCA and MnO_2 nanosheets to RAW264.7 cells. b) Percentage of LDH leakage of RAW264.7 cells after different treatments at various concentrations for 24 h. The error bars represent variations among three independent measurements.

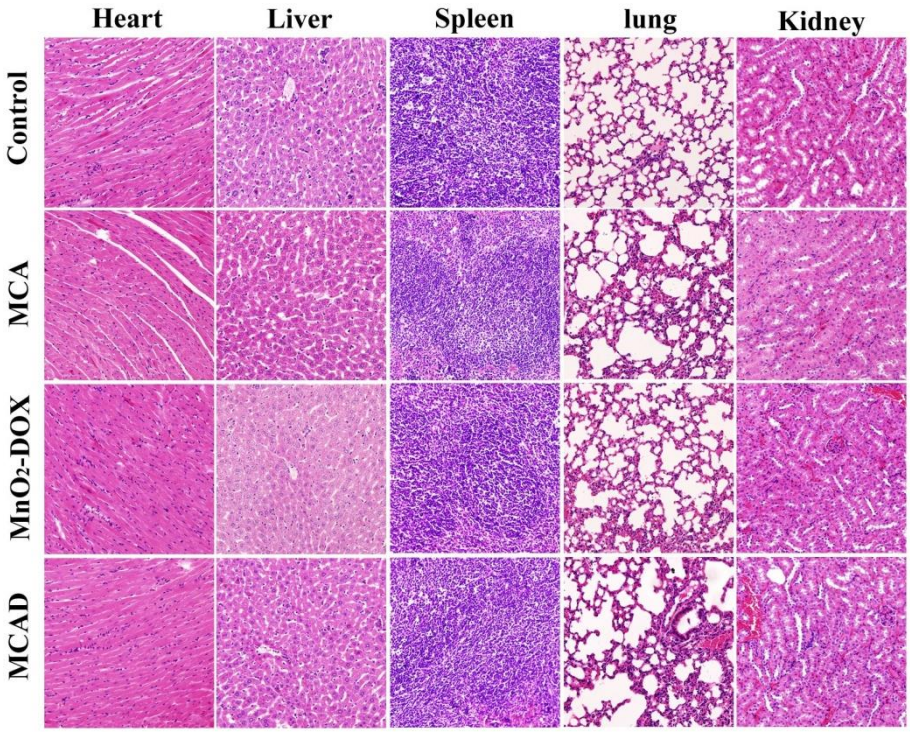

Fig. S22 H&E staining of major organs after 14 days of treatment with various nanomaterials. There was no obvious morphological change compared with the control group.

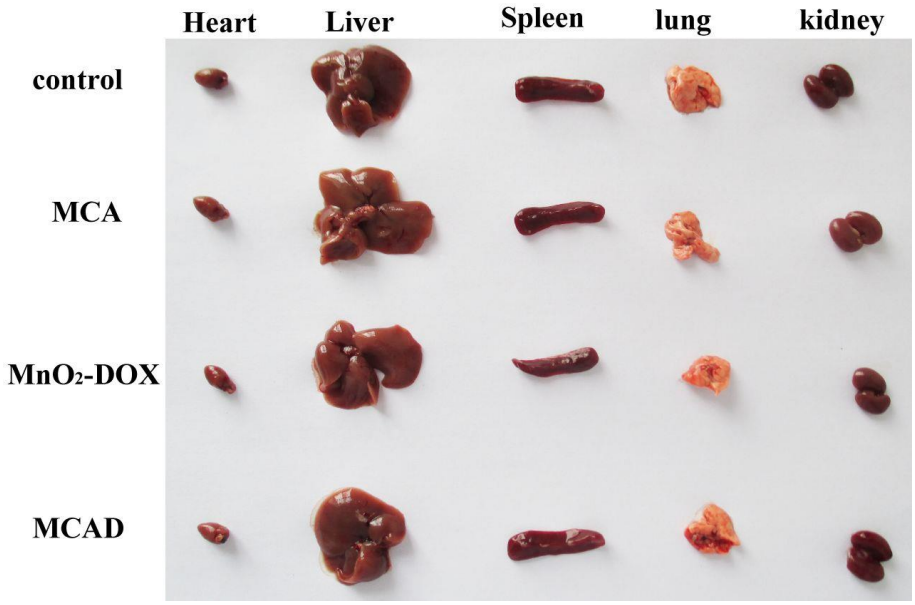

Fig. S23 Representative digital image of major organs after 14 days of treatment with various materials.

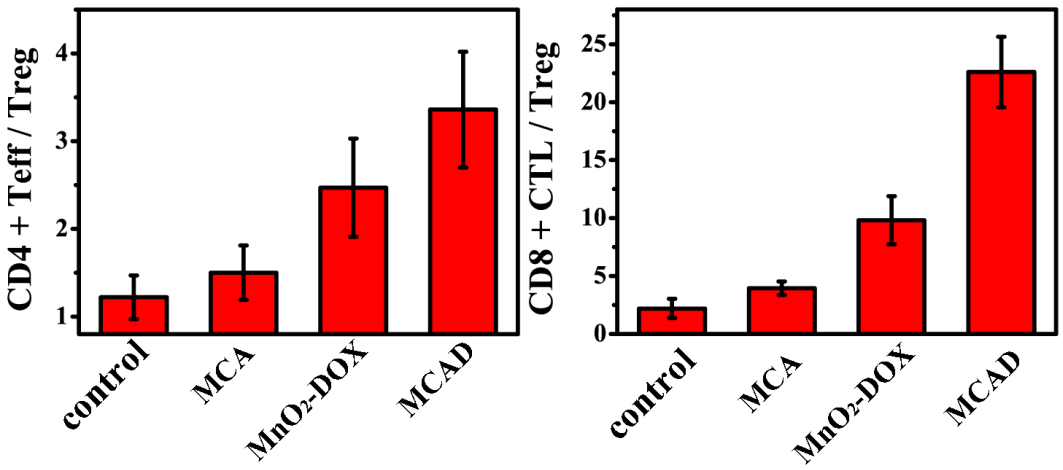

Fig. S24 Ratios of tumor-infiltrating effective $CD4^+$ T cells and $CD8^+$ T cells over regulatory T cells in tumors upon various treatments.